Available online at www.sciencedirect.com
ScienceDirect
Journal of Magnetic Resonance 188 (2007) 311–321
JMR Journal of Magnetic Resonance
www.elsevier.com/locate/jmr

# High-field $^{75}$As NMR study of arsenic oxysalts

Geoffrey M. Bowers *, R. James Kirkpatrick

*Department of Geology, University of Illinois at Urbana/Champaign, 1301 W. Green Street, Urbana, IL 61801, USA*

Received 18 June 2007; revised 16 July 2007
Available online 2 August 2007

**Abstract**

Arsenic is an important environmental hazard, but there have been few NMR investigations of its molecular scale structure and dynamics, due principally to the large quadrupole moment of $^{75}$As and consequent large quadrupole couplings. We examine here the potential of existing, single-field solid-state NMR technology to investigate solids containing arsenate and arsenite oxyanions. The results show that current techniques have significant potential for arsenates that do not contain both protonated $H_xAsO_4^{-(3-x)}$ groups and structural water molecules, but that the quadrupole couplings for the arsenites examined here are large enough that interpretation of the spectra is difficult, even at 21.1 T. Compounds that contain both structural $H_2O$ molecules and protonated arsenate groups do not yield resolvable signal, likely a result of $T_2$ effects related to a combination of strong quadrupolar interactions and proton exchange. Spin-echo experiments at 11.7 and 14.1 T were effective for $Li_3AsO_4$ and $CsH_2AsO_4$, as were whole-pattern spikelet experiments for arsenate oxide ($As_2O_5$) at 17.6 and 21.1 T. The central transition resonance of $Ca_3(AsO_4)_2{\cdot}8H_2O$ is ~6 MHz broad and required a non-conventional, histogram-style spikelet method at high field to improve acquisition efficiency. This approach reduces the acquisition time due to the sensitivity enhancement of the spikelet sequence and a reduction in the number of frequency increments required to map the resonance. Despite the large quadrupole couplings, we have identified a correlation between the $^{75}$As isotropic chemical shift and the electronegativity of the next-nearest neighbor cation in arsenate compounds.
© 2007 Elsevier Inc. All rights reserved.

*Keywords:* Arsenic; Histogram; QCPMG; Shielding; Solid-state nuclear magnetic resonance

## 1. Introduction

Arsenic (bio)geochemistry is of intense current interest because the speciation, mobility, and natural chemical processes involving arsenic compounds are intimately related to its bioavailability and a myriad of negative health effects related to arsenic exposure. Arsenic contamination in the environment is wide-spread due to the historical use of arsenic-bearing chemicals in agriculture and industry as well as the occurrence of natural and anthropogenic arsenic-rich waters in such regions as Bangladesh, South America, and the western United States [1–5]. A number of recent papers and news briefs have focused on the as yet poorly understood release of arsenic from arsenical-treated lumber [6–9]. This source is a significant current threat in the Gulf coast of the United States due the abundance of scrap lumber left in the wake of Hurricane Katrina [6,9] and the lack of regulations regarding disposal of arsenic-treated wood. Mobile forms of arsenic are also discharged to the environment from smelting operations, coal-burning power plants, and, historically, lumber treatment facilities and the use of arsenic-based pesticides and herbicides [10–12]. The toxicity of arsenic is well established, with chronic exposure to sub-ppm levels linked to skin cancer, arteriosclerosis and other cardiovascular diseases, myocardial infarction, chronic liver disease, Raynaud's syndrome, and potential teratogenic effects [4,11,13,14]. The principal sinks for arsenic in the environment are the soil clay fraction and eventually marine sediments [11,12,15–19]. It is therefore critical to develop

* Corresponding author. Fax: +1 217 244 4996.
*E-mail address:* gbowers@uiuc.edu (G.M. Bowers).

1090-7807/$ - see front matter © 2007 Elsevier Inc. All rights reserved.
doi:10.1016/j.jmr.2007.07.005

a fundamental understanding of arsenic–mineral relationships at the microscopic and macroscopic levels to aid in the design of arsenic remediation methods and the development of reactive transport models.

The speciation and chemistry of arsenic in the environment have been studied for decades, and it is known that the most commonly encountered forms are the oxyanions of arsenate (As(V)) and arsenite (As(III)) and various methylated versions of these species [11,20–22]. There have been several recent studies of arsenic binding on iron oxides and iron-rich minerals using X-ray absorption spectroscopy [23–28] and molecular modeling [29,30], but very little is known about the molecular-scale structural interactions between arsenate or arsenite and iron-poor soil minerals, and there is almost no information regarding the dynamical behavior of these species in environmentally relevant situations. Solid-state NMR is uniquely capable of probing local structure and the relatively slow dynamics often encountered in hydrous systems, but the extremely large $^{75}$As quadrupolar couplings reported to date [31–33] make arsenic NMR a traditionally unattractive approach. There have been several $^{75}$As nuclear quadrupole resonance (NQR) studies of minerals [34–37], but NQR does not readily yield the quadrupolar asymmetry parameter or chemical shielding, both of which can be important structural probes. Because the very broad peaks lead to poor sensitivity, most previous $^{75}$As NMR studies of solids have focused on synthetic semiconductor materials and crystalline compounds of relatively high symmetry [38–42]. However, Hari and colleagues [31–34,43,44] have reported $^{75}$As NMR data for chalcogenide glasses ($As_2Se_3$ and $As_2S_3$) and arsenite oxide ($As_2O_3$), some of which have quadrupolar couplings greater than 50 MHz as determined by NQR [33]. To circumvent the sensitivity and instrumentation difficulties associated with acquiring NMR resonances from these materials, Hari and co-workers implemented a stepped-field echo approach to collect histograms of the $^{75}$As powder patterns [44]. Their method offers significant reduction in data acquisition time compared to conventional whole-pattern echo acquisition and also relaxes demands on the probe tuning range. However, it has the significant drawback of requiring a spectrometer/magnet arrangement in which the field is controllable, readily varied, and capable of reaching very high homogeneity and field strength.

Here, we apply more conventional single-field NMR approaches to examine whether existing technologies can be successfully used to characterize structure and dynamics in arsenate and arsenite materials. Spin-echo, quadrupolar Carr–Purcell–Meiboom–Gill (QCPMG or spikelet sequence) whole-pattern, and a relatively easily implemented constant field, histogram acquisition spikelet approach are used to examine a series of arsenate and arsenite compounds. These approaches are quite successful for crystalline compounds bearing arsenate oxyanions but reveal significant obstacles for arsenite and protonated $H_xAsO_4^{-(3-x)} \cdot yH_2O$ materials. We discuss the successes and failures, benefits and limitations of the histogram spikelet approach, and relationships between arsenate isotropic chemical shielding and local structure. To the best of our knowledge, this is the first published NMR investigation of salts containing arsenate and arsenite oxyanions, the first to examine $^{75}$As chemical shielding in systems other than cubic GaAs [40], and the first instance where a histogram-style QCPMG approach is used to efficiently acquire extremely broad central transition NMR spectra.

## 2. Experimental

### 2.1. Materials and sample preparation

Samples of arsenic(V) oxide ($As_2O_5$), $NaAsF_6$, $Li_3AsO_4$, $CsH_2AsO_4$, $Ca_3(AsO_4)_2$, and $Na_2HAsO_4{\cdot}7H_2O$ were purchased from Alpha-Aesar. Arsenic (III) oxide ($As_2O_3$) and sodium arsenite ($NaAsO_2$) were purchased from Sigma–Aldrich. The purity of each sample was analyzed with X-ray diffraction using Cu-K$\alpha$ radiation on a Rigaku Geigerflex D Max-b diffractometer in the Materials Research Laboratory, a United States Department of Energy facility at the University of Illinois at Urbana-Champaign. Sharp reflections were obtained over the range from 10° to 70° 2$\theta$ using a scan rate of 12° per minute. The available powder instrumentation does not allow for control of the sample chamber atmosphere, and it proved impossible to obtain a good pattern from $Na_2HAsO_4{\cdot}7H_2O$ due to rapid moisture uptake. The other patterns demonstrated that each sample was pure, except $Ca_3(AsO_4)_2$ (which arrived as an octahydrate rather than the anhydrous form), $As_2O_5$ (which had low levels of $(H_3AsO_4)_2{\cdot}H_2O$; likely hydration of particle surfaces), and lithium arsenate, which is a mixture of $LiAsO_3$ and $Li_3AsO_4$. All samples were used as-received and stored under vacuum in a dessicator over mixed $CaSO_4$ and $Ca_3(PO_4)_2$ dessicants to limit moisture uptake. Samples for NMR analysis were packed into one inch long, 5 or 4 mm outer diameter glass NMR tubes in a glove bag under a dry $N_2$ atmosphere. The tubes were sealed with water-tight epoxy and stored in secondary vessels before being removed from the glove bag and analyzed in-house or at Pacific Northwest National Laboratory (PNNL), where the high-field NMR spectra were collected.

### 2.2. Spin-echo NMR experiments

It is well known that wide-line NMR spectra are frequently distorted in Bloch-decay experiments due to the loss of early data points in the FID during instrument ring-down. Thus, spin-echo NMR spectra were acquired for $CsH_2AsO_4$ and the mixed $Li_3AsO_4/LiAsO_3$ using the 11.7 T standard-bore Tecmag Aries and 14.1 T wide-bore Varian Infinity Plus spectrometers located at the University of Illinois. On the 14.1 T instrument, data were acquired using a Chemagnetics 4 mm double-resonance T3 probe with the transmitter set to +35 kHz from the reference fre-

quency. The reference was set using a 0.1 M aqueous solution of $NaAsF_6$, where the dominant interaction is a 1 kHz As–F scalar coupling [45]. Each data set involved 512 acquisitions of 2048 complex data points with a 200 kHz spectral width, inter-pulse delays of 50 and 45 μs (before and after the refocusing pulse, respectively), a transient delay of one second, and a central transition selective π/2 pulse width of 4 μs (obtained from the liquid state pulse width assuming a scaling of $I + 1/2$). Spectra were processed by left-shifting the data set by three points so that the initial data point corresponds to an echo maximum, zero-filling to 8192 data points, and applying the equivalent of 500 Hz of Lorenzian apodization prior to Fourier transformation.

Experiments on the 11.7 T instrument were performed using a home-built single-resonance probe with the transmitter set to +45 kHz from the reference frequency. In this case and for experiments at 17.1 and 21.1 T, the reference frequency and pulse width were obtained from solid $NaAsF_6$, which possess nearly perfect octahedral symmetry at the arsenic site and yields an NMR resonance dominated by dipolar and scalar couplings. Experiments on the 14.1 T instrument demonstrated that the π/2 pulse width obtained from solid $NaAsF_6$ is equivalent to the central transition selective pulse width calculated from the liquid-state π/2 pulse. The single-resonance probe and 11.7 T spectrometer were substantially less sensitive than the 14.1 T spectrometer and each data set involved 8192 acquisitions of 2048 complex data points with the remaining spectral parameters identical to the 14.1 T experiments. Spectra were processed by left-shifting the first ten data points and by applying the equivalent of 500 Hz of Lorenzian apodization prior to Fourier transformation.

### 2.3. Full-pattern spikelet NMR experiments

QCPMG experiments [46–49] were collected for $As_2O_5$ over the full central and partial satellite powder patterns using the 17.6 T Varian Unity Plus and 21.1 T Varian Inova spectrometers at Pacific Northwest National Laboratory. The experiments at 17.6 T used a single resonance static probe of a ''parallel'' tune design that offers a tuning range of approximately 50 MHz centered at the reference frequency. Data were acquired at this field using a spectral width of 1 MHz, acquisition delay of two seconds, and inter-pulse delays of 50 and 53 μs (before and after the inversion pulses, respectively). These inter-pulse delays were found experimentally to yield an echo maximum at the first acquisition point. One hundred inversion pulses were applied to acquire 128 transients at each of 108 transmitter frequencies, which were varied in 30 kHz increments. This spacing was found to minimize distortions in the combined spectrum due to the tuning and excitation profiles. Two hundred complex data points were acquired between echo maxima, leading to a frequency spacing of 5 kHz between spikes in the powder pattern. No apodization was applied to the data before Fourier transformation, although some zero and first order phase correction was required at most transmitter frequencies. The results from individual data sets were assembled using a sky-projection algorithm [50] to produce the overall resonance.

On the 21.1 T instrument, data for $As_2O_5$ were acquired using a TR probe modified to function in a single-resonance mode, which provided a tuning range of 16 MHz. The experimental conditions were identical to those on the 17.6 T instrument, except that the π/2 pulse length was 4.5 μs, the filter bandwidth was 400 kHz, and the inter-pulse delays were 50 and 55 μs, respectively. No signal was obtained for $Na_2HAsO_4{\cdot}7H_2O$ over a period of 40,000 transients at the reference frequency, in agreement with lower-field work in our lab that is not presented here. Again, 128 transients were acquired at each of 80 transmitter frequencies (separated by 40 kHz frequency increments) and combined with a sky projection algorithm to map out the powder pattern of $As_2O_5$. The slightly larger frequency step size led to small distortions in the assembled line-shape, and thus the data at 17.6 T was used for fitting to yield the most accurate NMR parameters.

### 2.4. Histogram spikelet NMR experiments

A novel histogram-style spikelet approach was used to acquire the spectra of $Ca_3(AsO_4)_2{\cdot}8H_2O$, $As_2O_3$, and $NaAsO_2$ at 17.6 T. This method involves movement of the transmitter frequency to provide a histogram of spikelet manifolds acquired using the QCPMG sequence and offers additional reduction in acquisition time over the variable-field echo method of Hari and colleagues [44] via the well-documented sensitivity enhancement of spikelet NMR [46,49,51–53]. It also retains the time savings of a histogram-style acquisition scheme and can be applied using conventional NMR hardware. The pulse widths, delays, and associated QCPMG conditions used in the histogram spikelet experiments were identical to those for $As_2O_5$ at 17.6 T described above. All the histogram spikelet experiments were performed at 17.6 T due to the larger probe tuning bandwidth compared to the 21.1 T probe. The transmitter frequency was initially incremented in 1 MHz intervals until the high- and low-frequency edges of the resonance were identified. The frequency interval was then narrowed until enough histogram points were obtained to enable a reasonable level of uncertainty in the spectral parameters extracted from calculated line-shapes; typically, good quality was achieved with 25–30 histogram points. For most samples a transmitter frequency spacing of one MHz was adequate, but it proved necessary to use 250 kHz for $Ca_3(AsO_4)_2{\cdot}8H_2O$ due to the comparatively narrower line-width. A complete central transition spectrum was collected for $Ca_3(AsO_4)_2{\cdot}8H_2O$, but the resonances of $As_2O_3$ and $NaAsO_2$ exceeded the tuning range of the parallel tune probe. The individual spikelet envelopes were combined with a sky projection algorithm in Octave, the GNU version of Matlab, to produce the overall resonances. Each spikelet data set received 2000 Hz of

Table 1
Best fit $^{75}$As NMR parameters extracted from iterative simulation of the experimental spectra

| Sample/resonance | $C_q$ (MHz) | $\eta_q$ | $\delta_{iso}$ (ppm) | $\delta_{aniso}$ (ppm) | $\eta_{cs}$ |
|---|---|---|---|---|---|
| $Li_3AsO_4$ | 2.85 ± 0.10 | 1.0 ± 0.05 | 384 ± 8 | — | — |
| $CsH_2AsO_4$ | 5.12 ± 0.22 | 0.05 ± 0.05 | 367 ± 5 | −49 ± 20 | 1 ± 0.1 |
| $As_2O_5$—Tet. As | 21.3 ± 0.2 | 0.38 ± 0.07 | 273 ± 28 | — | — |
| $As_2O_5$—Oct. As | 17.5 ± 0.4 | 1.0 ± 0.05 | 0 ± 10 | — | — |
| $Ca_3(AsO_4)_2{\cdot}8H_2O$ | 57 ± 1 | 0.74 ± 0.04 | 779 ± 300 | — | — |

comb-filter apodization prior to Fourier transformation and sky projection.

### 2.5. Spectral simulations

The quadrupolar and chemical shift parameters were extracted from the experimental spectra via line-shape simulations with SIMPSON [54]. For $CsH_2AsO_4$, $As_2O_5$, and $Ca_3(AsO_4)_2{\cdot}8H_2O$, echo spectra were calculated using ideal pulses and 17,710 or 317,810 weighted crystallite orientations prepared with the Zaremba–Conroy–Wolfsburg method [55,56]. The $LiAsO_3/Li_3AsO_4$ simulations were performed in a similar fashion using 8000 crystallite orientations prepared with the REPULSION method [57]. A quantitative estimate of the uncertainty in each parameter was determined by comparing the visual best-fit parameters to those calculated using SIMPLEX iterative simulations in SIMPSON for all but the $Ca_3(AsO_4)_2{\cdot}8H_2O$. In the latter compound, the spectral parameters obtained from the histogram spikelet spectra were compared to parameters determined by iteratively fitting the spikelet intensities as a function of frequency in DMFit [58]. Table 1 contains a summary of the NMR parameters and their uncertainties extracted for each of the arsenic resonances analyzed here.

## 3. Results

The $^{75}$As NMR spectrum of $CsH_2AsO_4$ contains a single resonance with a relatively small quadrupolar coupling constant of 5.13 MHz, a very low asymmetry parameter, and an isotropic shift of 367 ppm, in the tetrahedral $^{75}$As region (Fig. 1 and Table 1). $CsH_2AsO_4$ has tetragonal symmetry and contains a single tetrahedral arsenic site [59,60], in agreement with our NMR observations. However, quadrupolar interactions alone do not adequately position the so-called "magic angle" feature in the powder pattern appearing at roughly 33 kHz [61], suggesting some contribution of chemical shift anisotropy (CSA) to the line shape. The inclusion of a relatively small CSA of −26 ppm (reported here as the reduced anisotropy defined in the Haeberlen convention [62]) with an assumed asymmetry of 1.0 and a principal axis system oriented identically to the quadrupolar interaction positions this feature correctly (Fig. 2). The essentially null quadrupolar asymmetry parameter indicates that the electric-field gradient at the arsenic site is at least axially symmetric, as expected based on the tetragonal symmetry of $CsH_2AsO_4$ and the doubly

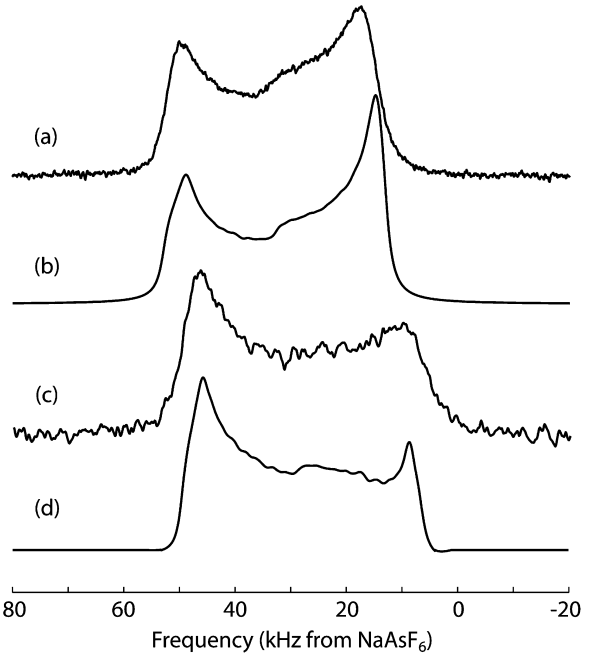


Fig. 1. $^{75}$As NMR spectra of $CsH_2AsO_4$ from 14.1 T (a and b) and 11.7 T (c and d). Spectra (b) and (d) are the best fit iterative simulation results.

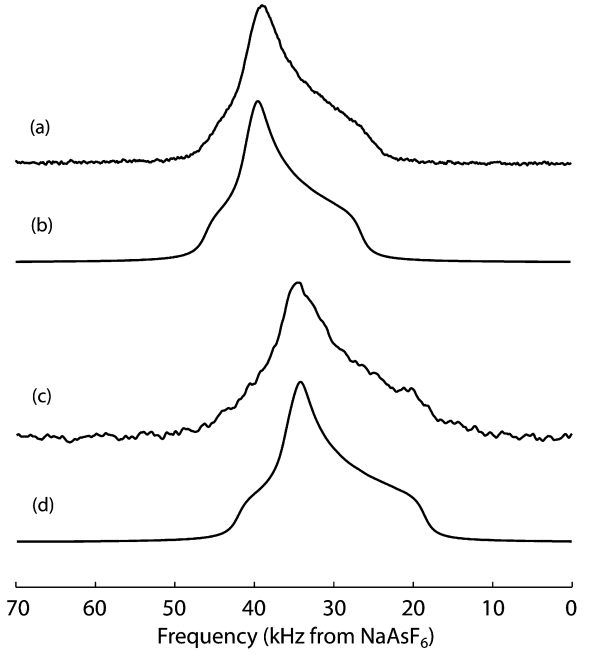


Fig. 2. $^{75}$As NMR spectra of $Li_3AsO_4$ from 14.1 T (a and b) and 11.7 T (c and d). Spectra (a) and (c) are the experimental data, (b) and (d) the individual best-fit lines.

protonated orthoarsenate groups [59,60,63]. It is reasonable to expect some influence of $^{1}H$–$^{75}As$ dipolar coupling as well, since two single-spin couplings of 1692 Hz (calculated based on the neutron diffraction H–As distance of 2.3 Å [60]) are similar in magnitude to the CSA. Given that the 4 kHz CSA only shifts the central singularity by a few kHz without significantly affecting any other aspect of the line-shape, it is reasonable to expect that the dipolar coupling is too small to cause a line-shape alteration. It is likely that dipolar coupling contributes only to spectral line-broadening, as suggested by the quality fit involving only CSA and a quadrupolar interaction. Simulations incorporating dipolar coupling also did not alter the reported parameters or the calculated line-shape to a significant extent. The observed deviations of the experimental spectra from the calculated shapes is an effect of the rf-field strength (31 kHz), which ideally should be 25 kHz (50% of the line-width) to yield an undistorted spectrum [64,65]. In the 11.7 T spectrum, the simulated resonance incorporates ideal pulses to account for the distortion of the low-field singularity due to the rf-field strength. For this reason, the parameters reported in Table 1 are derived from the 14.1 T data.

The $Li_3AsO_4$ sample, which XRD analysis shows to contain nearly equal amounts of $Li_3AsO_4$and $LiAsO_3$, yields relatively narrow NMR resonances at both 11.7 and 14.1 T using spin-echo methods (Fig. 2). These spectra are well fit by single, quadrupole-dominated patterns involving a large asymmetry parameter (Table 1). This is somewhat surprising because $Li_3AsO_4$ and $LiAsO_3$ have orthorhombic and monoclinic symmetries, respectively, and both contain a single $AsO_4$ site [66–68] with different distributions of As–O bond distances and tetrahedral neighbors. The observed spectrum suggests that the arsenic environments in these materials are not sufficiently different to yield unique spectra, that the two sites are completely overlapped at these fields, or that only one of the two sites is observed under this set of experimental conditions. It seems unlikely that the first explanation is valid given the discrepancy in As–O bond lengths ($Li_3AsO_4$: 1.551, 1.551, 1.563, and 1.569 Å; $LiAsO_3$: 1.594, 1.609, 1.727, and 1.806 Å). It is also unlikely that the two resonances overlap, as the fit quality is high at both fields assuming a single high-asymmetry quadrupolar resonance. It is more likely that the $Li_3AsO_4$ site with the smaller bond length distribution is being observed and that the $LiAsO_3$ resonance is not visible above the noise in 512 transients. Note that the bond lengths of $Li_3AsO_4$ do not define an axially symmetric site, allowing for the large asymmetry parameter. The resonance for $Li_3AsO_4$ exhibits a positive isotropic chemical shift with respect to octahedrally coordinated arsenic in $NaAsF_6$, as expected from, for instance, the well-known positive shifts of tetrahedral $^{27}Al$ and $^{29}Si$ relative to octahedral coordination [69,70]. The NMR parameters are reported based on the 14.1 T data in Table 1.

The spectrum for $As_2O_5$ is so broad that it cannot be adequately obtained with Bloch-decay methods, but the spectrum constructed from the 17.6 T QCPMG data is of good quality (Fig. 3). It contains three singularities in the central-transition region, consistent with the presence of multiple quadrupole-dominated arsenic environments. The featureless intensity observed at high frequency extends many MHz outside the plot window in both directions and is associated with the satellite transitions. The best fit of the central transition region was obtained with two pure quadrupolar resonances having the parameters presented in Table 1. $As_2O_5$ contains one tetrahedrally coordinated arsenic site and one octahedrally coordinated arsenic site of equal abundances linked by bridging oxygen atoms [71]. Based on the well-known shielding effects of increased coordination by oxygen for other nuclei (for example, $^{27}Al$), we assign the resonance with an isotropic chemical shift of 0 ppm to octahedral arsenic and the one at 270 ppm to tetrahedral arsenic. The sum of the calculated spectra in Fig. 3 achieved a best fit with a 0.95/1 tetrahedral/octahedral atomic ratio, very close to the abundance predicted from the X-ray crystal structure.

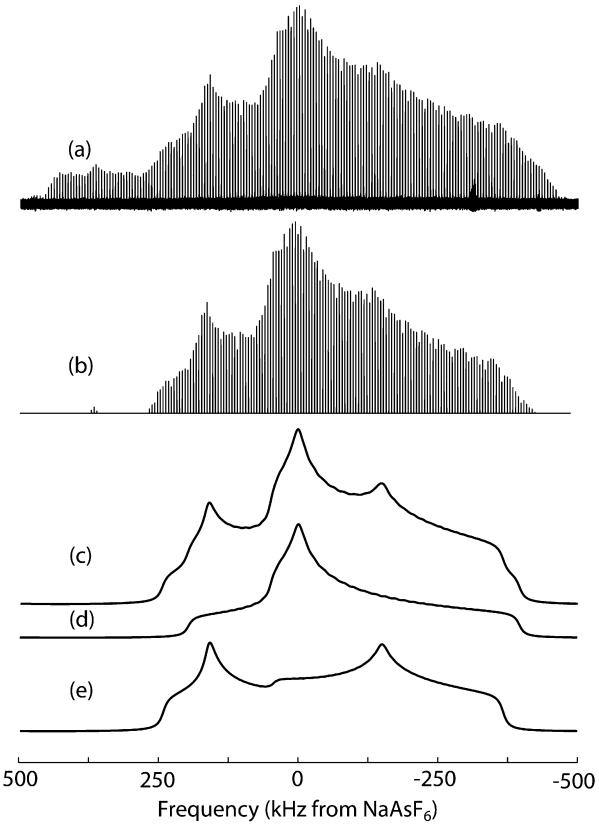


Fig. 3. The central one MHz region of the $^{75}As$ NMR spectrum of $As_2O_5$ acquired at 17.6 T (a). Spectrum (b) is the central transition region only and (c) is the simulated resonance combining the contributions of the octahedral (d) and tetrahedral (e) sites.

The spectrum of $Ca_3(AsO_4)_2{\cdot}8H_2O$ (Fig. 4) is even broader than that of $As_2O_5$ but was readily acquired with the histogram-style QCPMG experiment. The results highlight the balance between acquisition time and the number of data points needed for accurate simulations of histogram-spikelet spectra. The spectrum with a 500 kHz fre-

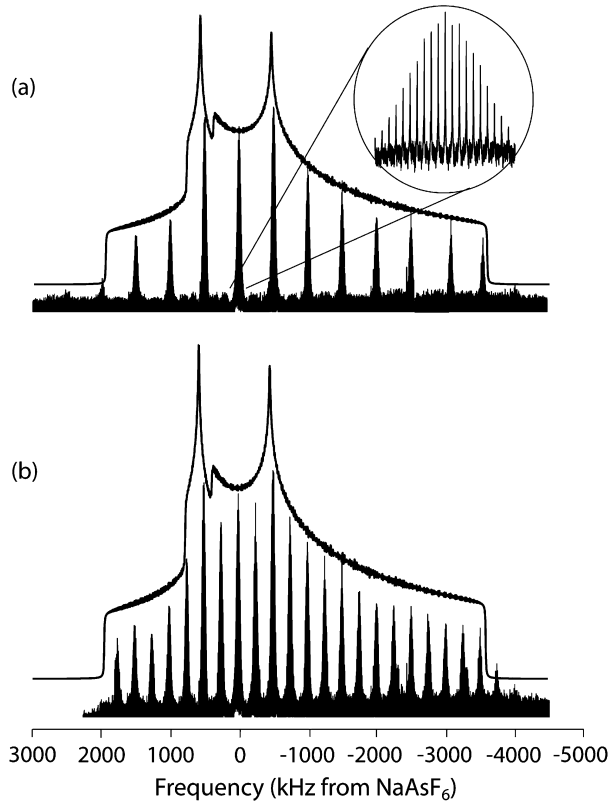


Fig. 4. $^{75}$As histogram spikelet spectra and simulated echo spectra of $Ca_3(AsO_4)_2{\cdot}8H_2O$ acquired with a 500 kHz frequency increment (a) and a 250 kHz frequency increment (b). The inset shows that each histogram point is composed of an individual spikelet manifold with a 5 kHz spikelet spacing.

quency increment has adequate data points to demonstrate the presence of a quadrupolar-dominated resonance but yields parameters with a relatively high degree of uncertainty compared to the histogram spikelet spectrum acquired with a 250 kHz frequency increment (for example, the uncertainty in the chemical shift is 400 ppm versus 300 ppm, respectively, as determined in DMFit). However, the spectrum with a 250 kHz increment requires double the acquisition time, which may not be feasible in samples with lower sensitivity. The best fit to both data sets was obtained assuming only a single quadrupole-dominated resonance and an isotropic chemical shift of 779 ppm (Table 1). There is no clear evidence of significant anisotropic shielding, although the inherent uncertainty of histogram-style acquisition prevents us from firmly ruling out some contribution to the line shape. The isotropic chemical shift of 779 ppm confirms structural refinement data that the arsenic is in tetrahedral coordination [72] and shows that the chemical shift range of tetrahedral $^{75}$As is as large as 500 ppm.

For arsenite in $As_2O_3$ and $NaAsO_2$, even the histogram spikelet approach using the parallel tune probe with a 50 MHz tuning range at 17.6 T does not yield complete spectra due to the very large quadrupole couplings. For $As_2O_3$, we are able to observe the low-frequency edge of the $^{75}$As resonance (Fig. 5), because no detectable signal

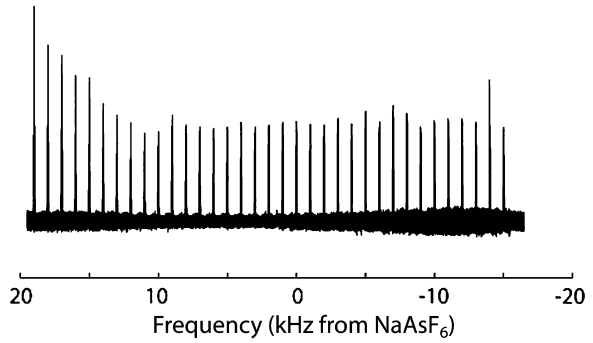


Fig. 5. Partial $^{75}$As NMR spectrum of $As_2O_3$ obtained at 17.6 T.

is obtained with the transmitter set below −15 MHz, which is well within our tuning range. However, the signal extends in the opposite direction to the high-frequency tuning limit of +20 MHz (central transition width of 35 MHz). The observed resonance is highly distorted and does not possess a classical quadrupolar line-shape, suggesting that the full resonance was not obtained under these conditions. Treacy and Taylor report a quadrupole coupling for crystalline $As_2O_3$ of roughly 118 MHz using NQR [35], suggesting that the central transition NMR line-width will be on the order of 60 MHz and confirming that histogram spikelet NMR with the tuning setup used here is not appropriate for $As_2O_3$. For $NaAsO_2$, neither the low-frequency nor high-frequency edge of the resonance could be detected, meaning the central transition is in excess of 50 MHz in width and information regarding the chemical shift cannot be obtained. In the absence of a probe with a broader tuning range, the variable-field histogram approach is the only currently available NMR method for studying arsenite compounds that do not possess high symmetry.

## 4. Discussion

### *4.1. The histogram-style spikelet approach: benefits and limitations*

The results presented here, combined with previously published NMR and NQR results for $^{75}$As, clearly illustrate the advantages and disadvantages of the histogram-style spikelet approach for nuclei with broad central transition resonances. For central transition (CT) widths in the 10 s of kHz range (QCC ~0 to 6 MHz for $^{75}$As), spin-echos are adequate and readily implemented, as illustrated by the spectra for $Li_3AsO_4$ and $CsH_2AsO_4$ (Figs. 1 and 2). For CT line-widths in the 100 s of kHz to MHz range, the QCPMG sequence provides sufficient sensitivity enhancement to enable efficient acquisition in most cases, although the histogram spikelet approach may slightly decrease the required acquisition time toward the high end of this range. When the CT line-width is between 2 and 3 MHz up to the full tuning range of the probe, the histogram spikelet scheme provides significant time savings

relative to conventional whole-pattern QCPMG. By not acquiring intensity uniformly across the CT, the acquisition time is reduced by a factor directly proportional to the applied transmitter increment and inversely proportional to the transmitter increment that yields a smooth whole-pattern spectrum. For our $Ca_3(AsO_4)_2{\cdot}8H_2O$ data at 17.6 T, there is a time savings of 250 kHz/30 kHz ≈8-fold versus whole-pattern acquisition with QCPMG.

The histogram spikelet method also benefits from the sensitivity enhancing properties of the QCPMG sequence. The signal-to-noise enhancement for QCPMG relative to a conventional echo experiment as given by Lefort et al. [53] is:

$$S/N_{\text{gain}} = 2\nu_{\text{QCPMG}}\sqrt{T_2 \cdot T_{\text{off}}}$$

where $\nu_{\text{QCPMG}}$ is the frequency spacing between spikelets in Hz, $T_2$ is the true transverse relaxation time, and $T_{\text{off}}$ is the time in which the signal appears to decay to zero in a single half-echo FID. For the spikelet conditions employed for $Ca_3(AsO_4)_2{\cdot}8H_2O$, and assuming values of 18 ms for $T_2$ and 20 μs for $T_{\text{off}}$ (based on the appearance of the free induction decay), the signal-to-noise ratio enhancement is ~6.0 compared to conventional echo acquisition.

Thus, for our histogram-style spikelet spectrum of $Ca_3(AsO_4)_2{\cdot}8H_2O$, the overall reduction in signal-to-noise ratio is approximately one order of magnitude compared to whole-pattern Hahn-echo acquisition, equivalent to an acquisition time savings of two to three orders of magnitude once combined with the benefits of histogram acquisition. It is also worth noting that some of the other sensitivity enhancement methods typically applied to quadrupolar nuclei, including double frequency sweep [73] and rotor assisted population transfer [74], are not generally applicable to $^{75}$As NMR or other nuclei with very large quadrupole moments. This is because central transition resonances many MHz in width make it difficult to invert or saturate the satellites due to the large frequency span of the central and satellite transitions and the quality factor of the NMR probe. Some additional sensitivity enhancement could be achieved by decreasing the temperature of the sample/probe/electronics (at the expense of longer relaxation times unless paramagnetic dopants are employed) and/or by cross-polarization from protons in protonated arsenate/ite oxyanions, provided the proton dynamics are slow enough [50]. Equipment access prevented such investigations during this study.

While the frequency histogram spikelet method is more readily implemented than the variable-field based method of Hari et al. [44], it is limited by the tuning range of the probe. Constant-field spectrometers are much more common that those with well controlled variable fields, but many common probe designs have relatively narrow tuning ranges. For example, the 16 MHz tuning range of the triple-resonance 5 mm probe for the 21.1 T instrument at PNNL proved to be inadequate for obtaining the full spectra of the two arsenite oxyanion compounds examined here. The 50 MHz range of the parallel tune probe on the 17.6 T instrument is more suitable for constant-field histogram spikelet experiments, but even it was incapable of acquiring the full resonance of the arsenites without changing the tuning configuration. The variable-field histogram approach does not place such stringent demands on probe tuning and electronics, and it and NQR remain the methods of choice for central transitions with linewidths >50 MHz.

Another limitation involves the inherent uncertainty of the histogram approach to acquisition. Given the large frequency jumps that would be common for situations where histogram spikelet NMR is suitable, the maximum uncertainty can be quite high. For example, in a histogram spikelet spectrum of a quadrupolar nucleus like $^{75}$As, the total width of the resonance is directly related to the quadrupolar coupling constant and is known only to a certainty of twice the frequency increment (the maximum error on the high- and low-frequency edges) minus four times the half-width of each spikelet manifold. Likewise, the position of the singularities that reveal the quadrupolar asymmetry parameter are either contained in one of the spikelet manifolds or located between two spikelet manifolds. The maximum error in the position of the singularities is then one frequency increment minus twice the half-width of an individual spikelet manifold. A similar argument can be made about the isotropic chemical shift. For the $Ca_3(AsO_4)_2{\cdot}8H_2O$, the maximum error in the line-width is thus 840 kHz for the 500 kHz spacing spectrum and 340 kHz for the 250 kHz spacing spectrum and the maximum errors in the position of the singularities are 420 and 170 kHz, respectively. In practice, all three parameters can be identified with greater certainty given the added restraint of the well-known expression for the quadrupolar frequency shift (see Table 1), which defines clear relationships between the NMR parameters. These uncertainties compare favorably to those of Hari and colleagues. One should note that the isotropic chemical shift is identified with the least accuracy in the case of $Ca_3(AsO_4)_2{\cdot}8H_2O$.

### 4.2. $^{75}$As chemical shift correlations

The results here show that $^{75}$As chemical shifts for arsenate oxides and oxyanions correlate with nearest and next-nearest atomic structure and composition in ways analogous to other cations, including $^{27}$Al, $^{29}$Si, $^{31}$P, and $^{77}$Se [70,75–78]. Changes in nearest neighbor coordination cause quite large variations in the isotropic chemical shift, as expected. Six-coordinate $^{75}$As(V) in $As_2O_5$ resonates near 0 ppm, in agreement with previously published results [40,45], whereas tetrahedral $^{75}$As(V) resonates at significantly more positive values. For the four tetrahedral sites characterized in the arsenate compounds we examined, there is a roughly 500 ppm chemical shift range, indicating that the isotropic chemical shift for this coordination reflects structure and composition at greater than nearest neighbor distances. There is a quite good

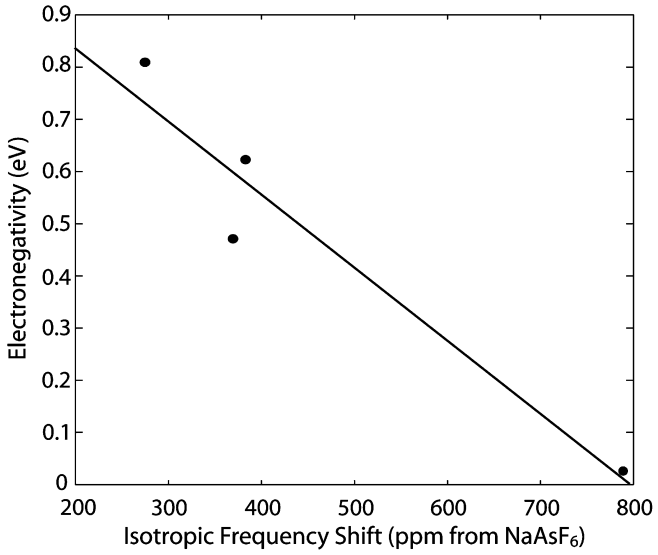


Fig. 6. The linear correlation between $^{75}$As chemical shift and the electronegativity of the next nearest neighbor cations. The line corresponds to the equation $y = -0.0014x + 1.128$.

($R^2 = 0.927$) linear correlation between the isotropic chemical shift and the Pauling electronegativity [79] of the next nearest neighbor cations in the arsenate oxyanion materials (Fig. 6). Note that the outlier represents the $CsH_2AsO_4$ compound, suggesting that the two protonated oxygen atoms also exert some influence on the $^{75}$As chemical shift; NMR of additional protonated species is necessary to fully explore possible protonation state-chemical shift trends. There is no clear relationship between isotropic chemical shift and next nearest neighbor cation size, charge, or ionic radius. These results imply that a detectable change in the isotropic chemical shift will occur for an arsenate oxyanion when the next nearest neighbor structure changes; for example, during the nucleation or crystallization of an arsenate-bearing precipitate or sorption of arsenate oxyanion by a mineral. Clearly, the isotropic chemical shift is an important parameter for detailed, molecular-level structure studies of arsenates using $^{75}$As magnetic resonance techniques.

### *4.3. Impact of hydration and oxyanion protonation on $^{75}$As NMR*

For $Na_2HAsO_4{\cdot}7H_2O$, it was not possible to observe any $^{75}$As NMR signal above background at 14.1 T or 21.1 T. The structure of this phase can be characterized as tubes of Na atoms coordinated octahedrally by water molecules with $HAsO_4^{-2}$ groups located at the center of the tubes [80]. The absence of detectable signal could be due to (a) strong static $^1$H–$^{75}$As dipolar couplings leading to very large linewidths, (b) a large $^{75}$As quadrupolar coupling for $HAsO_4^{-2}$ groups leading to very large linewidths, or (c) fluctuations of the arsenic electric-field gradient due to proton exchange between protonated arsenate groups and water molecules leading to substantial lifetime ($T_2$) broadening. As discussed above, the relatively high arsenic resonance frequency permits $^1$H–$^{75}$As dipolar couplings of >10 kHz at inter-nuclear distances of less than 1.2 Å, but at the As–H internuclear distance for protonated arsenate (~2.4 Å), the dipolar coupling is of the order of 1500 Hz and not large enough to cause substantial broadening. A very large quadrupolar coupling due to oxyanion protonation seems unlikely, since we observe a $^{75}$As resonance with a relatively small quadrupolar interaction for the $H_2AsO_4^-$ groups in crystalline $CsH_2AsO_4$. However, it should be noted that the symmetry of $H_2AsO_4^{-1}$ is different from $HAsO_4^{-2}$, and thus a large quadrupolar interaction cannot be ruled out entirely. Due to the large quadrupole moment of $^{75}$As, lifetime broadening due to EFG fluctuations caused by exchange of protons between $HAsO_4^{-2}$ and $H_2O$ is the most likely explanation. Water molecules occur as nearest neighbors to the protonated arsenate oxyanion in $Na_2HAsO_4{\cdot}7H_2O$ with the three-dimensional structure preserved via a regular hydrogen bonding network [80–82]. The hydrogen bonding network will almost certainly contain vacancies that permit proton hopping between structural waters and the arsenate groups. EFG fluctuation due to proton exchange is also supported by the observation that $^{75}$As NMR signal for $H_xAsO_4^{-(3-x)}$ anions cannot be detected in aqueous solution at pHs less than the value required to fully deprotonate the arsenate tetrahedra [83]. Many arsenic–mineral systems occur under conditions where water is present, and these results suggest that structural and dynamical studies of arsenic sorbed to soil minerals will be very challenging using current NMR methods.

## 5. Conclusions

The results presented here show that the $^{75}$As chemical shift range for arsenate oxides and oxyanions is broad and sensitive to local coordination number and electronegativity of the next nearest neighbor species. Existing NMR methods can be useful in investigating arsenate oxyanions in simple crystalline solids, and the histogram-style spikelet experiments are quite useful for obtaining extremely broad resonances efficiently with reasonable accuracy in the quadrupolar parameters. The large quadrupolar couplings in arsenite compounds make $^{75}$As NMR of As(III) materials extremely difficult at a single magnetic field. It was impossible to observe $^{75}$As signal for compounds containing both protonated arsenate groups and structural water molecules, probably a result of $T_2$ effects related to EFG fluctuations due to rapid $^1$H exchange between the protonated oxyanions and neighboring water molecules. We conclude that the primary challenges to $^{75}$As NMR in environmental systems will be (i) to slow or eliminate the effect of $^1$H motion while maintaining environmentally relevant conditions and (ii) obtain a high enough concentration of sorbed $^{75}$As to enable efficient detection with field- or frequency-histogram spikelet experiments.

## Acknowledgments

This research was supported by the United States Department of Energy, Office of Basic Science, grant number DE-FG01-05ER05010201. All spectra reported here were acquired in the High Field Magnetic Resonance User facility, located in the William R. Wiley Environmental and Molecular Sciences Laboratory at Pacific Northwest National Laboratory.

## References

[1] M.G.M. Alam, G. Allinson, F. Stagnitti, A. Tanaka, M. Westbrooke, Arsenic contamination in Bangladesh groundwater: a major environmental and social disaster, International Journal of Environmental Health Research 12 (2002) 235–253.
[2] A.S.M. Kamal, P. Parkpian, Arsenic contamination in Hizla, Bangladesh: sources, effects and remedies, Science Asia 28 (2002) 181–189.
[3] M. Khalequzzaman, F.S. Faruque, A.K. Mitra, Assessment of arsenic contamination of groundwater and health problems in Bangladesh, International Journal of Environmental Research and Public Health 2 (2005) 204–213.
[4] J.M. Borgono, P. Vicent, H. Venturino, A. Infante, Arsenic in drinking water of city of Antofagasta—epidemiological and clinical study before and after installation of a treatment-plant, Environmental Health Perspectives 19 (1977) 103–105.
[5] P.D. Whanger, P.H. Weswig, J.C. Stoner, Arsenic levels in Oregon waters, Environmental Health Perspectives 19 (1977) 139–143.
[6] E. Engelhaupt, Arsenic in Katrina's wood debris, Environmental Science & Technology 40 (2007), News Brief.
[7] K. Stook, T. Tolaymat, M. Ward, B. Dubey, T. Townsend, H. Solo-Gabriele, G. Bitton, Relative leaching and aquatic toxicity of pressure-treated wood products using batch leaching tests, Environmental Science & Technology 39 (2005) 155–163.
[8] B.I. Khan, J. Jambeck, H.M. Solo-Gabriele, T.G. Townsend, Y. Cai, Release of arsenic to the environment from CCA-treated wood. 2. Leaching and speciation during disposal, Environmental Science & Technology 40 (2006) 994–999.
[9] B. Dubey, H.M. Solo-Gabriele, T.G. Townsend, Quantities of arsenic-treated wood in demolition debris generated by Hurricane Katrina, Environmental Science & Technology 41 (2007) 1533–1536.
[10] F.X.X. Han, Y. Su, D.L. Monts, M.J. Plodinec, A. Banin, G.E. Triplett, Assessment of global industrial-age anthropogenic arsenic contamination, Naturwissenschaften 90 (2003) 395–401.
[11] W.R. Cullen, K.J. Reimer, Arsenic speciation in the environment, Chemical Reviews 89 (1989) 713–764.
[12] L.M. Walsh, M.E. Sumner, D.R. Keeney, Occurrence and distribution of arsenic in soils and plants, Environmental Health Perspectives 19 (1977) 67–71.
[13] V. Bencko, Carcinogenic, teratogenic, and mutagenic effects of arsenic, Environmental Health Perspectives 19 (1977) 179–182.
[14] L.M. Walsh, D.R. Keeney, Behavior and phytotoxicity of inorganic arsenicals in soils, in: Arsenical Pesticides, American Chemical Society, Washington, DC, 1975.
[15] R.S. Braman, Arsenic in the environment, in: Arsenical Pesticidesl, American Chemical Society, Washington, D.C., 1975.
[16] E.A. Crecelius, R. Carpenter, Arsenic distribution in waters and sediments of the Puget Sound region, in: First Annual NSF Trace Contaminants Conference. Oak Ridge National Laboratory, Oak Ridge, Tennessee, 1973.
[17] G. Lunde, Occurrence and transformation of arsenic in marine environment, Environmental Health Perspectives 19 (1977) 47–52.
[18] E.A. Woolson, Fate of arsenicals in different environmental substrates, Environmental Health Perspectives 19 (1977) 73–81.
[19] L. Arcon, J.T. van Elteren, H.J. Glass, A. Kodre, Z. Slejkovec, EXAFS and XANES study of arsenic in contaminated soil, X-ray Spectrometry 34 (2005) 435–438.
[20] E.A. Crecelius, Changes in chemical speciation of arsenic following ingestion by man, Environmental Health Perspectives 19 (1977) 147–150.
[21] F.H. Zhao, D.Y. Ren, B.S. Zheng, T.D. Hu, T. Liu, Modes of occurrence of arsenic in high-arsenic coal by extended X-ray absorption fine structure spectroscopy, Chinese Science Bulletin 43 (1998) 1660–1663.
[22] A. Violante, M. Ricciardella, S. Del Gaudio, M. Pigna, Coprecipitation of arsenate with metal oxides: nature, mineralogy, and reactivity of aluminum precipitates, Environmental Science & Technology 40 (2006) 4961–4967.
[23] A.L. Foster, G.E. Brown, G.A. Parks, T.N. Tingle, D.E. Voigt, S.L. Brantley, XAFS determination of As(V) associated with Fe(III) oxyhydroxides in weathered mine tailings and contaminated soil from California, USA, Journal De Physique Iv 7 (1997) 815–816.
[24] B.C. Bostick, S. Fendorf, Arsenite sorption on troilite (FeS) and pyrite ($FeS_2$), Geochimica et Cosmochimica Acta 67 (2003) 909–921.
[25] S. Dixit, J.G. Hering, Comparison of arsenic(V) and arsenic(III) sorption onto iron oxide minerals: implications for arsenic mobility, Environmental Science and Technology 37 (2003) 4182–4189.
[26] B. Cances, F. Juillot, G. Morin, V. Laperche, L. Alvarez, O. Proux, J.L. Hazemann, G.E. Brown, G. Calas, XAS evidence of As(V) association with iron oxyhydroxides in a contaminated soil at a former arsenical pesticide processing plant, Environmental Science & Technology 39 (2005) 9398–9405.
[27] G. Ona-Nguema, G. Morin, F. Juillot, G. Calas, G.E. Brown, EXAFS analysis of arsenite adsorption onto two-line ferrihydrite, hematite, goethite, and lepidocrocite, Environmental Science & Technology 39 (2005) 9147–9155.
[28] C.M. Su, R.T. Wilkin, Arsenate and arsenite sorption on and arsenite oxidation by iron(II, III) hydroxycarbonate green rust, in: Advances in Arsenic Research, 2005, pp. 25–40.
[29] K.A. Matis, M. Lehmann, A.I. Zouboulis, Modelling sorption of metals from aqueous solution onto mineral particles: the case of arsenic ions and goethite ore, NATO Science Series, Series E: Applied Sciences 362 (1999) 463–472.
[30] J.D. Kubicki, Comparison of As(III) and As(V) complexation onto Al- and Fe-hydroxides, in: Advances in Arsenic Research, 2005, pp. 104–117.
[31] P. Hari, S. Guzel, T. Su, P.C. Taylor, P.L. Kuhns, W.G. Moulton, N.S. Sullivan, Photodarkening effect in glassy $As_2S_3$and $As_2O_3$, Journal of Non-Crystalline Solids 326 (2003) 199–204.
[32] P. Hari, T. Su, P.C. Taylor, P.L. Kuhns, W.G. Moulton, N.S. Sullivan, Photodarkening in glassy $As_2S_3$, Journal of Non-Crystalline Solids 266 (2000) 929–932.
[33] P.C. Taylor, P. Hari, A. Kleinhammes, P.L. Kuhns, W.G. Moulton, N.S. Sullivan, Asymmetries in local bonding sites in amorphous semiconductors: very high field NMR of As-75, Journal of Non-Crystalline Solids 230 (1998) 770–774.
[34] P.C. Taylor, T. Su, P. Hari, E. Ahn, A. Kleinhammes, P.L. Kuhns, W.G. Moulton, N.S. Sullivan, Structural and photostructural properties of chalcogenide glasses: recent results from magnetic resonance measurements, Journal of Non-Crystalline Solids 326 (2003) 193–198.
[35] D.J. Treacy, P.C. Taylor, Nuclear quadrupole resonance in two crystalline forms of arsenic trioxide, arsenolite and claudetite I, Solid State Communications 40 (1981) 135–138.
[36] I.N. Pen'kov, I.A. Safin, Nuclear quadrupole resonance (N.Q.R.) in orpiment, Doklady Akademii Nauk SSSR, 156 (1964) 139–41.
[37] I.N. Pen'kov, Nature of traces structural impurities in some chalcogenides of arsenic, antimony, and bismuth from nuclear quadrupole resonance data, Geokhimiya (1971) 731–742.
[38] M. Suemitsu, N. Nakajo, Charged point defects in GaAs crystals evaluated by nuclear-magnetic resonance spin echo, Journal of Applied Physics 66 (1989) 3178–3186.

[39] L.D. Potter, Y. Wu, NMR measurements of homonuclear indirect couplings in GaAs, Journal of Magnetic Resonance A 116 (1995) 107–112.
[40] L.D. Potter, A.A. Guzelain, A.P. Alivisatos, Y. Wu, Structure of chemically synthesized nanophase GaAs studies by nuclear magnetic resonance and X ray diffraction, Journal of Chemical Physics 103 (1995) 4834–4840.
[41] J. Takeuchi, H. Nakamura, H. Yamada, E. Kita, A. Tasaki, T. Erata, Quadrupolar nutation NMR on a compound semiconductor gallium arsenide, Solid State Nuclear Magnetic Resonance 8 (1997) 123–128.
[42] R.W. Schurko, S. Wi, L. Frydman, Dynamic effects on the powder line shapes of half-integer quadrupolar nuclei: a solid-state NMR study of $XO_4^-$ groups, Journal of Physical Chemistry A 106 (2002) 51–62.
[43] T. Su, P. Hari, E. Ahn, P.C. Taylor, P.L. Kuhns, W.G. Moulton, N.S. Sullivan, Asymmetries of local arsenic bonding sites in $As_xS_{1-x}$ and $As_xSe_{1-x}$ glasses, Physical Review B 67 (2003).
[44] P. Hari, P.C. Taylor, A. Kleinhammes, P.L. Kuhns, W.G. Moulton, N.S. Sullivan, Asymmetry in the local structural order in arsenic chalcogenide glasses: high field NMR in crystalline and glassy $As_2Se_3$, Solid State Communications 104 (1997) 669–672.
[45] G. Baliman, P.S. Pregosin, As-75 nuclear magnetic resonance study of some arsenic salts, Journal of Magnetic Resonance 26 (1977) 283.
[46] J.T. Cheng, P.D. Ellis, Adsorption of rubidium($1^+$) to γ-alumina as followed by solid-state rubidium-87 NMR spectroscopy, Journal of Physical Chemistry 93 (1989) 2549–2555.
[47] S.E. Shore, J.P. Ansermet, C.P. Slichter, J.H. Sinfelt, NMR study of the bonding and diffusion of Co chemisorbed on Pd, Physical Review Letters 58 (1987) 953–956.
[48] A.N. Garroway, Homogeneous and inhomogeneous nuclear spin echoes in organic solids: adamantane, Journal of Magnetic Resonance (1969–1992) 28 (1977) 365–371.
[49] F.H. Larsen, H.J. Jakobsen, P.D. Ellis, N.C. Nielsen, Sensitivity-enhanced quadrupolar-echo NMR of half-integer quadrupolar nuclei. Magnitudes and relative orientation of chemical shielding and quadrupolar coupling tensors, Journal of Physical Chemistry A 101 (1997) 8597–8606.
[50] A.S. Lipton, J.A. Sears, P.D. Ellis, A general strategy for the NMR observation of half-integer quadrupolar nuclei in dilute environments, Journal of Magnetic Resonance 151 (2001) 48–59.
[51] R.W. Schurko, I. Hung, C.M. Widdifield, Signal enhancement in NMR spectra of half-integer quadrupolar nuclei via DFS-QCPMG and RAPT-QCPMG pulse sequences, Chemical Physics Letters 379 (2003) 1–10.
[52] G.M. Bowers, A.S. Lipton, K.T. Mueller, High-field QCPMG NMR of strontium nuclei in natural minerals, Solid State Nuclear Magnetic Resonance 29 (2006) 95–103.
[53] R. Lefort, J.W. Wiench, M. Pruski, J.P. Amoureux, Optimization of data acquisition and processing in Carr–Purcell–Meiboom–Gill multiple quantum magic angle spinning nuclear magnetic resonance, Journal of Chemical Physics 116 (2002) 2493–2501.
[54] M. Bak, J.T. Rasmussen, N.C. Nielsen, SIMPSON: a general simulation program for solid-state NMR spectroscopy, Journal of Magnetic Resonance 147 (2000) 296–330.
[55] S.K. Zaremba, Good lattice points, discrepancy, and numerical integration, Annali di Matematica Pura ed Applicata 4–73 (1966) 293.
[56] H. Conroy, Molecular schrodinger equation 8. A new method for evaluation of multidimensional integrals, Journal of Chemical Physics 47 (1967) 5307.
[57] M. Bak, N.C. Nielsen, REPULSION, a novel approach to efficient powder averaging in solid-state NMR, Journal of Magnetic Resonance 125 (1997) 132–139.
[58] D. Massiot, F. Fayon, M. Capron, I. King, S. Le Calve, B. Alonso, J.-O. Durand, B. Bujoli, Z. Gan, G. Hoatson, Modeling one- and two-dimensional solid-state NMR spectra, Magnetic Resonance in Chemistry 40 (2002) 70–76.
[59] A. Ferrari, M. Nardelli, M. Cingi, Cesium orthoarsenates, Gazzetta Chimica Italiana 86 (1956) 1174–1180.
[60] J.W. Hay, R.J. Nelmes, Structural studies of deuterated $CsH_2AsO_4$ in its paraelectric and ferroelectric phases, Journal Of Physics C-Solid State Physics 14 (1981) 1043–1052.
[61] B.C. Gerstein, C.R. Dybowski, Transient Techniques in NMR of Solids: An Introduction to Theory and Practice, Academic Press, Orlando, Fla., 1985.
[62] U. Haeberlen, High resolution NMR in solids: Selective averaging, in: J.S. Waugh (Ed.), Advances in Magnetic Resonance, Supplement 1, Academic Press, New York, 1976.
[63] V.I. Pakhomov, G.B. Sil'nitskaya, G.K. Semin, V.A. Gerken, I.I. Kalashnikova, Structural perfection of cesium hydrogen arsenate ($CsH_2AsO_4$) crystals, Izvestiya Akademii Nauk SSSR, Neorganicheskie Materialy 21 (1985) 158–159.
[64] E. Van Veenendaal, B.H. Meier, A.P.M. Kentgens, Frequency stepped adiabatic passage excitation of half-integer quadrupolar spin systems, Molecular Physics 93 (1998) 195–213.
[65] A.P.M. Kentgens, A practical guide to solid-state NMR of half-integer quadrupolar nuclei with some applications to disordered systems, Geoderma 80 (1997) 271–306.
[66] V.J. Zemann, Die Kristallstruktur von Lithiumphosphat, $Li_3PO_4$, Acta Crystallographica 13 (1960) 863.
[67] A.R. West, F.P. Glasser, Preparation and crystal chemistry of some tetrahedral lithium phosphate-type compounds, Journal of Solid State Chemistry 4 (1972) 20–28.
[68] H. von Waltraud, K. Dornberger-Schiff, Die Kristallstruktur von lithiumpolyarsenat $(LiAsO_3)_x$, Acta Crystallographica 9 (1956) 87–88.
[69] J.F. Stebbins, M. Kanzaki, Local structure and chemical shifts for six-coordinated silicon in high-pressure mantle phases, Science (Washington, DC, United States) 251 (1991) 294–298.
[70] D. Mueller, W. Gessner, A.R. Grimmer, Determination of the coordination number of aluminum in solid aluminates from the chemical shift of aluminum-27, Zeitschrift fuer Chemie 17 (1977) 453–454.
[71] M. Jansen, Crystal structure of $As_2O_5$, Angewandte Chemie 16 (1977) 314–315.
[72] R. Gopal, C. Calvo, Crystal structure of calcium arsenate(v), Canadian Journal of Chemistry 49 (1971) 1036–1046.
[73] A.P.M. Kentgens, Quantitative excitation of half-integer quadrupolar nuclei by a frequency-stepped adiabatic half-passage, Journal of Magnetic Resonance 95 (1991) 619–625.
[74] H.T. Kwak, S. Prasad, Z. Yao, P.J. Grandinetti, J.R. Sachleben, L. Emsley, Enhanced sensitivity in RIACT/MQ-MAS NMR experiments using rotor assisted population transfer, Journal of Magnetic Resonance 150 (2001) 71–80.
[75] X.Q. Hou, R.J. Kirkpatrick, Solid-state Se-77 NMR and XRD study of the structure and dynamics of seleno-oxyanions in hydrotalcite-like compounds, Chemistry of Materials 12 (2000) 1890–1897.
[76] E.R. Andrew, A. Bradbury, R.G. Eades, G.J. Jenks, Fine structure of the nuclear magnetic resonance spectra of solids. Chemical shift structure of the spectrum of phosphorus pentachloride, Nature (London, United Kingdom) 188 (1960) 1096–1097.
[77] J. Sanz, J. Serratosa, $^{29}Si$ and $^{27}Al$ high-resolution MAS-NMR spectra of phyllosilicates, Journal of the American Chemical Society 106 (1984) 4790–4793.
[78] R.A. Kinsey, R.J. Kirkpatrick, J. Hower, K.A. Smith, E. Oldfield, High-resolution Al-27 and Si-29 nuclear magnetic resonance spectroscopic study of layer silicates, including clay minerals, American Mineralogist 70 (1985) 537–548.
[79] D.R. Lide (Ed.), CRC Handbook of Chemistry and Physics, seventy-ninth ed., CRC Press, Boca Raton, 1998.
[80] G. Ferraris, D.W. Jones, J. Yerkess, Neutron diffraction study of the crystal structure of sodium arsenate heptahydrate, $Na_2HAsO_4{\cdot}7H_2O$, Acta Crystallographica, Section B: Structural Crystallography and Crystal Chemistry 27 (1971) 354–359.
[81] W.H. Baur, A.A. Khan, Crystal chemistry of salt hydrates. VI. Crystal structures of disodium hydrogen orthoarsenate heptahydrate and of disodium hydrogen orthophosphate heptahydrate, Acta

Crystallographica, Section B: Structural Crystallography and Crystal Chemistry 26 (1970) 1584–1596.

[82] G. Ferraris, G. Chiari, Crystal structure of disodium hydrogen orthoarsenate heptahydrate, $Na_2HAsO_4{\cdot}7H_2O$, Acta Crystallographica, Section B: Structural Crystallography and Crystal Chemistry 26 (1970) 1574–1583.

[83] U.G. Nielsen, J. Majzlan, J. Kim, K. Julmis, D. Clinton, C.P. Grey, Local environment in defect iron soil minerals and ion sorption on iron oxyhydroxides studied by solid-state NMR spectroscopy, Abstracts of Papers, 232nd ACS National Meeting, San Francisco, CA, United States, Sept. 10–14, 2006, (2006) COLL-422.